




Article

A Cu₁₂ Metallacycle Assembled from Four C₃-Symmetric Spin Frustrated Triangular Units

Basharat Ali ^{1,2}, Grégoire David ³, Frédéric Gendron ³, Xiao-Lei Li ^{1,4} , Olivier Cador ³, Winfried Plass ⁵ , Boris Le Guennic ^{3,*}  and Jinkui Tang ^{1,2,*}

- ¹ State Key Laboratory of Rare Earth Resource Utilization, Changchun Institute of Applied Chemistry, Chinese Academy of Sciences, Changchun 130022, China; ali537@mail.ustc.edu.cn (B.A.); lixl@ciac.ac.cn (X.-L.L.)
- ² School of Applied Chemistry and Engineering, University of Science and Technology of China, Hefei 230026, China
- ³ Univ Rennes, CNRS, ISCR (Institut des Sciences Chimiques de Rennes)—UMR 6226, F-35000 Rennes, France; gregoire.david@univ-rennes1.fr (G.D.); frederic.gendron@univ-rennes1.fr (F.G.); olivier.cador@univ-rennes1.fr (O.C.)
- ⁴ Key Laboratory of Advanced Energy Materials Chemistry (Ministry of Education), College of Chemistry, Nankai University, Tianjin 300071, China
- ⁵ Institut für Anorganische und Analytische Chemie, Friedrich-Schiller-Universität Jena, D-07743 Jena, Germany; sekr.plass@uni-jena.de
- * Correspondence: boris.leguennic@univ-rennes1.fr (B.L.G.); tang@ciac.ac.cn (J.T.)

Abstract: Assembling metallacycles with interesting topological arrangements is a critical task for chemists. We report here a novel dodecanuclear Cu^{II} compound, $[\{\text{Cu}_3\text{L}(\mu\text{-N}_3)\}_4(\text{Py})_{14}] \cdot 2\text{Py}$ (**Cu₁₂**) (where Py = pyridine and $[\text{H}_6\text{L}]\text{Cl}$ = tris(2-hydroxybenzylidene)triaminoguanidinium chloride, respectively), with the topology of a cycle accomplished by four two-connecting approximately flat C₃-symmetric guanidine-based ligands. Each ligand affords three tridentate metal-binding cavities and the four node-to-node connections through single azido bridges are provided by pairs of metal centers. A theoretical investigation using CASSCF in addition to DFT calculations showed strong antiferromagnetic coupling within the Cu₃-triangles, resulting in spin-frustrated systems. However, these calculations were not able to properly reproduce the very weak antiferromagnetic couplings between the triangle units, highlighting the challenge of describing the magnetic behavior of this compound.

Keywords: spin frustration; copper triangles; metallacycle



Citation: Ali, B.; David, G.; Gendron, F.; Li, X.-L.; Cador, O.; Plass, W.; Le Guennic, B.; Tang, J. A Cu₁₂ Metallacycle Assembled from Four C₃-Symmetric Spin Frustrated Triangular Units. *Magnetochemistry* **2023**, *9*, 122. <https://doi.org/10.3390/magnetochemistry9050122>

Academic Editor: Carlos J. Gómez García

Received: 10 April 2023

Revised: 26 April 2023

Accepted: 3 May 2023

Published: 6 May 2023



Copyright: © 2023 by the authors. Licensee MDPI, Basel, Switzerland. This article is an open access article distributed under the terms and conditions of the Creative Commons Attribution (CC BY) license (<https://creativecommons.org/licenses/by/4.0/>).

1. Introduction

Coordination chemistry provides an opportunity for construction by self-assembling an apparently limitless variety of structures [1,2]. Specifically, the construction of the supramolecular coordination chemistry of transition metal complexes has received much attention over the last couple of decades, due to their vital roles in biology [3–5], catalysis [6,7], and more importantly, in magneto-chemistry [8–14]. In this context, polytopic threefold symmetric ligands based on triaminoguanidine are of particular interest in crystal engineering and supramolecular chemistry [15–18] due to their structural diversity and the chemical versatility of the resulting systems [19–24]. Ligands possessing triaminoguanidine core have been successfully employed to develop high-nuclear supramolecular cages, but with diamagnetic metal ions [2,25–29]. Only a couple of open-shell metal ion systems [30,31], copper(II) coordination polymers [32,33], and a series of trinuclear cobalt(II) [34], nickel(II) [35,36], Iron (III) [37], and copper(II) [38,39] triangles have been studied magnetically, with the latter two showing the phenomenon of spin frustration, having significant applications in molecular spintronics [40].

Triaminoguanidine-based ligands with three equivalent coordinating sites could coordinate with three metal ions, leading to an almost planar structure style and rather small metal···metal distances bridged through the N–N diazine channels of the central triaminoguanidine moiety [30]. Consequently, the established complexes display strong antiferromagnetic exchange interactions through the σ bond of the N–N diazine arms of the ligand and among the metal centers [34–36]. In this regard, Plass and co-workers [38,39] developed two trinuclear copper(II) triangles, $[\text{Cu}_3\text{L}(\text{py})_6]\text{ClO}_4$ (**Cu₃py**) and $[\text{Cu}_3\text{L}(\text{bpy})_3]\text{ClO}_4 \cdot 3\text{DMF}$ (**Cu₃bpy**) (py and bpy are pyridine and bipyridine, respectively). Both complexes exhibit strong antiferromagnetic coupling between the copper(II) ions, leading to a spin-frustrated system. Very recently, by fluctuating the synthetic approach while keeping the same metal–ligand combination, we synthesized two new antiferromagnetic hexa-nuclear Cu^{II} complexes, $[\text{Cu}_6\text{L}_2\text{Cl}(\mu\text{-OAc})(\text{DMF})_3] \cdot \text{DMF}$ (**Cu₆**) and $[\text{Cu}_6\text{L}_2(\mu\text{-Cl})_2(\text{DMF})_4]$ (**Cu₆Cl**), in which two planar triangles with strict C_3 -symmetry were deliberately bridged through acetate and chloride anions in *cis* and *trans* fashions, respectively [41]. It was assumed that both **Cu₆** and **Cu₆Cl** would also present the phenomenon of spin frustration based on their similar structural and experimental magnetic properties to the reference compounds, **Cu₃py** and **Cu₃bpy**.

Coordination supramolecular cages with tetrahedral topologies have been constructed using triaminoguanidine-based ligands, tris (2-hydroxybenzylidene) triaminoguanidinium $[\text{H}_6\text{L}]^+$, and tris (5-bromo-2-hydroxybenzylidene) triaminoguanidinium $[\text{H}_6\text{L}_1]^+$, in which the triangular units were connected through $(-\text{CdO}-)_2$ four-membered rings (O from the phenolate of the ligand itself), resulting in $[\{(\text{CdCl})_3\text{L}\}]^{8-}$ and $[\{(\text{CdCl})_3\text{L}_1\}]^{8-}$, respectively [28,42]. The authors concluded that the construction of a comparable discrete single-walled supramolecular tetrahedron with Zn^{2+} ions was impossible due to the much smaller size of the Zn^{2+} ion relative to the Cd^{2+} ion (Zn^{2+} , 0.74 Å; Cd^{2+} , and 0.97 Å) [29]. In the case of a Zn^{2+} single-walled tetrahedron, the triangular faces would result in closer contact in view of its smaller size, which is sterically unfavorable. Hence, based on this assumption, they developed a double-walled tetrahedron using two different triaminoguanidine-based mixed ligands [29]. Keeping this task in mind, this work planned to use an azide anion as a bridging co-ligand, owing to its linear structure and least steric hindrance. Surprisingly, we synthesized a dodecanuclear metallacycle based on a Cu^{2+} ion (0.73 Å), $[\{\text{Cu}_3\text{L}(\mu\text{-N}_3)\}_4(\text{Py})_{14}] \cdot 2\text{Py}$ (**Cu₁₂**), assembled from four C_3 -symmetric isosceles triangular faces in close contact. Furthermore, the experimental and theoretical magnetic calculations revealed very strong intra-triangular antiferromagnetic exchange interactions between the copper ions through the σ bond pathway of the N–N diazine channels of the ligand, very similar to that of the reference compounds, **Cu₃py** and **Cu₃bpy**. To our knowledge, this is the first example of a supramolecular **Cu₁₂** metallacycle based on triaminoguanidine ligands with four isosceles triangular sub-units that has been synthesized and studied magnetically.

2. Materials and Methods

2.1. Materials and General Information

Tris(2-hydroxybenzylidene)triaminoguanidinium chloride $[\text{H}_6\text{L}]\text{Cl}$ (Scheme S1) was synthesized according to the methods in the literature [28,29]. Sodium azide was purchased and used without further purification. The elemental analyses of C, H, and N were completed on a PerkinElmer 2400 analyzer. The powder X-ray diffraction analysis was achieved on a Burker-D8 advance diffractometer using $\text{Cu-K}\alpha$ ($\lambda = 1.5418$ Å) radiation at room temperature.

Synthesis of $[\{\text{Cu}_3\text{L}(\mu\text{-N}_3)\}_4(\text{Py})_{14}] \cdot 2\text{Py} \cdot 4[\text{CH}_3\text{OH}] \cdot 0.8[\text{H}_2\text{O}]$ (**Cu₁₂**)

Two freshly prepared solutions, copper(II) salt $\text{Cu}(\text{OAc})_2 \cdot 6\text{H}_2\text{O}$ (43.8 mg, 0.15 mmol) in 10 mL of methanol and ligand $[\text{H}_6\text{L}]\text{Cl}$ (22.6 mg, 0.05 mmol) in 5 mL of pyridine, were mixed slowly with continued stirring. Then, the sodium azide (0.013 mg, 0.2 mmol) dissolved in 1 mL of water was added dropwise. After 3 h of further stirring, the final solution was filtered out and put aside for slow evaporation. After three days, well-shaped

dark green cube-like crystals of Cu_{12} in a quantitative yield suitable for single crystal measurements were obtained. The elemental analysis (%) calcd for $\text{C}_{168}\text{H}_{140}\text{Cu}_{12}\text{N}_{52}\text{O}_{12}$: C: 52.52, H: 3.67, and N: 18.95; and found C: 52.54, H: 3.65, and N: 18.93.

2.2. Crystallography

The details of the crystal data and structure refinement parameters of the Cu_{12} are summarized in Table S1, while the obtained bond lengths and angles are given in Table S2. To measure the single crystals of the titled complex, they were mounted on glass fiber under a microscope and the diffractogram data were collected at 120 (2) K using a Bruker AXS D8 Venture single-crystal diffractometer equipped with graphite-monochromatized Mo $K\alpha$ ($\lambda = 0.71073 \text{ \AA}$) (Table S1). The drawing of the molecular structure and mean plane analysis were obtained using the DIAMOND (version 3.1) software. The structure was solved using direct methods and SHELXT and refined using full-matrix least-squares methods based on F2 (SHELXL) in the Olex2 package [43,44].

2.3. Magnetic Measurements

The magnetic susceptibility measurements were performed on a polycrystalline sample using a Quantum Design MPMS-XL7 SQUID magnetometer in the 2–300 K temperature range, equipped with a 7 T magnet. The diamagnetic corrections of the constituent atoms were determined from Pascal's constants [45].

2.4. Theoretical Calculations

Based on the wavefunction theory (WFT), using the OpenMolcas software package with the complete active space (CAS) self-consistent field (SCF) approach [46], the electronic structures and magnetic properties of each Cu center were first calculated [47]. This was achieved by replacing the eleven other Cu^{II} ions with diamagnetic Zn^{II} centers using the X-ray structures. In combination with the all-electron atomic natural orbital relativistically contracted basis set (ANO-RCC) [48,49], the calculations were first carried out at the scalar (SR) level using the second-order Douglas–Kroll–Hess scalar relativistic Hamiltonian [50–52]. The basis sets were contracted to the triple- ζ plus polarization (TZP) quality for the Cu (21s15p10d6f4g2h/6s5p3d2f1g) and Cl (17s12p5d4f2g/5s4p2d1f) atoms, as well as for the N and O atoms coordinated to the paramagnetic center (N, O = 14s9p5d3f2g/4s3p2d1f). The Zn atoms were treated with a double- ζ plus polarization (DZP) basis set (21s15p10d6f4g2h/5s4p2d1f), whereas the rest of the C, N, O, and H atoms were treated with a double- ζ basis set (C, N, O = 14s9p5d3f2g/3s2p; H = 8s4p3d1f/2s). By considering the five lowest spin-doublet states and an active space formed by 11 electrons spanning 11 orbitals, the state-average calculations were performed accordingly. These 11 orbitals contained five 3d orbitals of the Cu^{II} ion, five 3d' orbitals by considering the double-shell effect, and one ligand-centered orbital that could form a bonding σ interaction with the metal-centered orbitals. By using the restricted active space state interaction (RASSI) approach [53], spin-orbit coupling (SOC) was introduced afterwards via a state interaction within the basis of the spin-orbit free states. The EPR g -factors were calculated based on the Reference [54], as implemented in the RASSI module of OpenMolcas, whereas the magnetic susceptibility and magnetization were calculated using the Single-Aniso and Poly-Aniso modules of OpenMolcas, as detailed in Reference [55].

Using the Amsterdam Density Functional (ADF) software package [56–58], Kohn–Sham density functional theory (DFT) calculations were carried out to evaluate the magnetic coupling between the Cu^{II} centers. The calculations of the magnetic coupling constants were performed based on the X-ray structures, in which ten of the paramagnetic Cu^{II} atoms were replaced by diamagnetic Zn^{II} centers. Such a replacement produced a model system of two Cu^{II} centers with a spin of 1/2, leading to a triplet or a singlet spin state.

These calculations utilized the scalar all-electron zeroth-order regular approximation (ZORA) [59] in combination with the spin-unrestricted formalism. The hybrid functionals, PBE0 [60,61] (Perdew–Burke–Ernzerhof) with 25% of exact Hartree–Fock exchange (HFX),

B3LYP [62–65] (Becke, three-parameter Lee–Yang–Parr) with 20% of HFX, and B3LYP* [66] with 15% of HFX, were employed along with the triple- ζ polarized Slater-type orbital (STO) all-electron basis set, with one set of polarization function for all the atoms (TZP) [67].

The magnetic exchange coupling J was determined from broken symmetry (BS) calculations first proposed by Noodleman [68], in addition to the spin decontamination scheme from Yamaguchi [69,70],

$$J = 2 \frac{E_{BS} - E_T}{\langle \hat{S}^2 \rangle_T - \langle \hat{S}^2 \rangle_{BS}}$$

where E_{BS} and E_T are the energy of the BS configuration and the triplet state, respectively, and $\langle \hat{S}^2 \rangle_{BS}$ and $\langle \hat{S}^2 \rangle_T$ are the expectation values of the \hat{S}^2 operator.

The magnetic susceptibility of Cu_{12} was then calculated using the PolyAniso module, as implemented in the OpenMolcas package, with the following spin Hamiltonian,

$$\hat{H} = \mu_B \sum_i g_i \cdot \hat{S}_i \cdot B - \sum_{i,j} J_{ij} \cdot \hat{S}_i \cdot \hat{S}_j$$

where the magnetic moments and magnetic coupling constants of each Cu^{II} center were obtained from the WFT and DFT calculations, respectively. It is worth noting that the validity of such a computational strategy has been successfully confirmed on a related trinuclear copper(II) complex [39] and closely related Cu_6 and CuCl_6 complexes [41].

3. Results and Discussions

3.1. Crystal Structure of Cu_{12}

The structural data obtained for $[\{\text{Cu}_3\text{L}(\mu\text{-N}_3)\}_4(\text{Py})_{14}] \cdot 2\text{Py} \cdot 4[\text{CH}_3\text{OH}] \cdot 0.8[\text{H}_2\text{O}]$ (Cu_{12}) revealed that the complex crystallizes in the triclinic space group $P\bar{1}$. The unit cell contains one crystallographically independent dodeca-nuclear neutral complex $[\{\text{Cu}_3\text{L}(\mu\text{-N}_3)\}_4(\text{Py})_{14}]$ and two co-crystallized pyridine molecules (Figure 1, left and Figure S1). The supporting information provides the selected crystallographic data, bond lengths, and angles for Cu_{12} in Tables S1 and S2.

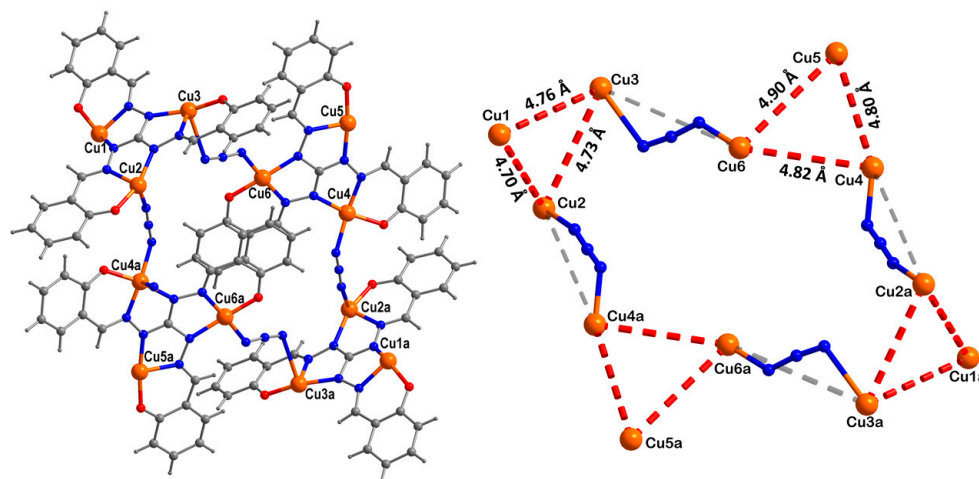


Figure 1. (left) Molecular structure of Cu_{12} , coordinated and solvent pyridine molecules have been omitted for clarity; and (right) triangular arrangements with calculated distances between the copper centers along with single-bridged mode (through azide anion) of four planar trinuclear units. Color code: orange, Cu; red, O; blue, N; grey, C; and light grey, H.

The asymmetric unit of Cu_{12} contains half of the molecule $[\{\text{Cu}_3\text{L}(\mu\text{-N}_3)\}_2(\text{Py})_7] \cdot \text{Py}$ (Figure S2). Each asymmetric unit contains two almost-planar C_3 -symmetric triangular fragments, which are bridged via Cu3 and Cu6 (6.11 Å) through azide anions (Figure 1, right and Figure S2). Finally, both asymmetric units are again node-to-node connected via Cu2 and Cu4 (5.95 Å) through azide anions to construct a dodeca-nuclear Cu_{12} metal-lacyle. In total, four two-connecting node-to-node connections via single azide bridges

are provided by pairs of metal centers (Figure 1, right). Within each triangle, the tri-topic ligand leads to an approximately planar symmetrical triangular arrangement through the N–N diazine bridges among the copper centers. In Cu1 to Cu5, all five copper centers are five-coordinated, in which three equatorial coordination sites (NNO) are occupied by the tridentate pockets of the ligand, along with two trapped pyridine molecules for both the Cu1 and Cu5 centers to provide trigonal bipyramid (D_{3h}) arrangements, while in the case of the Cu2 to Cu4 centers, the remaining two coordination sites are filled by one pyridine and one bridging azide anion to accomplish spherical square pyramid (C_{4v}) geometries, respectively (Figure S3 and Table S3). Cu6 is the only metal ion that is four-coordinated and whose fourth position is occupied by the bridging azide anion in cooperating with the planar tridentate pocket (NNO) of the ligand, displaying a square planar (D_{4h}) geometry (Figure S3). The distances within intra-triangular copper ions range between 4.70 Å and 4.90 Å (Figure 1 right). The Cu–N–N–Cu dihedral angles are almost linear, ranging from 147.32° to 177.97°. The calculated bond lengths and dihedral angles of **Cu₁₂** are very consistent with the reported spin-frustrated triangles, **Cu₃py** and **Cu₃bpy** [38,39].

In addition, at first glance, an offset face-to-face $\pi\cdots\pi$ interaction may exist between the two perfectly parallel benzene rings of the ligands related by an inversion center (Figure 2, left), proved by the short distance of 4.06 (1) Å between the centroids of the benzene rings. Although the vertical distance of 3.36 (4) Å between them corresponds to the formation of a weak $\pi\cdots\pi$ interaction between the benzene rings, the planes of the two adjacent benzene rings hardly overlap with each other at all, seeing that the centroid shift distance of 2.26 (9) Å between the two benzene rings is almost equal to the centroid distance of 2.42 (1) Å between the two adjacent side-by-side benzene rings (Figure 2, right). Thus, there was nearly no $\pi\cdots\pi$ interaction in the **Cu₁₂** and a further negligible exchange interaction attached to the centers of Cu6 and Cu6a can be transmitted along this path.

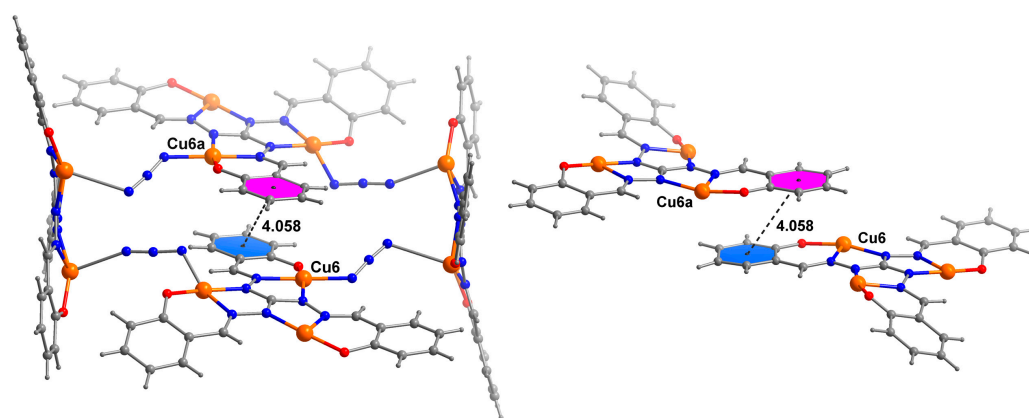


Figure 2. The view of the $\pi\cdots\pi$ stacking interaction within the **Cu₁₂** attached to the centers of Cu6 and Cu6a; the coordinated and solvent pyridine molecules have been omitted for clarity; the relative benzene rings were highlighted with purple and blue colors, respectively. Color code: orange, Fe; red, O; blue, N; grey, C; and light grey, H.

3.2. Magnetic Properties

Temperature-dependent direct current (dc) molar susceptibility ($\chi_M T$) measurements for **Cu₁₂** were performed in the temperature range of 2 to 300 K (Figure 3). The room temperature $\chi_M T$ value of 3.30 cm³ K mol^{−1} is significantly lower than the spin-only value expected for the twelve independent Cu^{II} ions ($\chi_M T = 0.375$ cm³ K mol^{−1} for $S = 1/2$ and $g = 2.0$). The $\chi_M T$ products decreased gradually with lowering the temperature, reaching a plateau value of about 1.8 cm³ K mol^{−1} at around 40 K. This behavior indicates strong antiferromagnetic interactions within the intra-triangular Cu^{II} ions, with a ground spin state of $S = 1/2$. Below 15 K, the $\chi_M T$ value dropped down sharply to reach a value of 1.51 cm³ K mol^{−1} at 2 K, indicating the existence of weak inter-triangular interactions between the four Cu₃ triangles in the **Cu₁₂** [34–36,38,39]. The field dependence of the

magnetization curve was also measured for Cu_{12} under 2.0 K between 0 and 70 kOe (Figure S4). The obtained magnetization plateau value was ca. $3.96 \mu_{\text{B}}$ at 70 kOe, which is consistent with the $S = 2$ spin ground state for the four triangular units (each with $S = 1/2$) and fully in line with the recently reported spin-frustrated triangles, Cu_3py and Cu_3bpy , based on the same ligand.

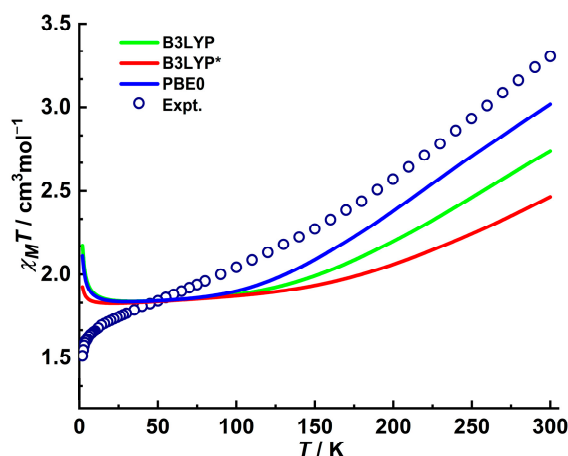


Figure 3. Calculated (solid lines) and experimental (empty circles) magnetic susceptibilities ($\chi_{\text{M}}T$) as a function of the temperature. Theoretical results are shown for magnetic couplings computed from DFT broken symmetry calculations using B3LYP (red), B3LYP* (green), and PBE0 (blue) functions. Magnetic moments of Cu^{II} are obtained with the CASSCF method. Details of calculations are presented in Tables S4–S6.

3.3. Theoretical Calculations

The calculated magnetic susceptibility obtained with the different density functionals and experimental data are reported in Figure 3. Between them, a relatively good qualitative agreement was reached for the high-temperature range. This resulted from a relevant determination of the strong antiferromagnetic intra-couplings (J_{intra}) between the Cu^{II} ions of the same triangular unit (Table S4). However, the couplings determined from the different functionals used in this work were not able to properly reproduce the trend of ($\chi_{\text{M}}T$) in the low-temperature range. The magnetic behavior at low temperatures mainly resulted from the interactions between the triangular units through the *cis* or *trans* azido bridges. These (J_{azido}) couplings were determined as very weakly ferromagnetic, with values in the order of magnitude of the cm^{-1} (Table S4). This order of magnitude is basically the expected accuracy of the DFT BS evaluation. Hence, one may have some doubts about the ability of this level of theory to properly evaluate these couplings. In addition, the magnetic couplings between copper ions mediated by such end-to-end azido bridges have been deeply investigated in the literature and are expected to be weakly antiferromagnetic [71–74]. However, using higher levels of theory such as WFT-based methods is untractable regarding the size of the system considered here.

In order to confirm the possible antiferromagnetic behavior of J_{azido} , we simulated the $\chi_{\text{M}}T$ curve using an average value of $J_{\text{intra}} = -250 \text{ cm}^{-1}$ and different values of J_{azido} . Presented in Figure 4, these results show that using a weak antiferromagnetic J_{azido} qualitatively allows the reproduction of the magnetic behavior of Cu_{12} , even at the low-temperature range. Using these different antiferromagnetic J_{azido} results in a non-magnetic ground state. The $\chi_{\text{M}}T$ product increased rapidly with respect to the temperature as the low-lying excited states were populated. For $J_{\text{azido}} = -2, -5, \text{ and } -15 \text{ cm}^{-1}$, the $\chi_{\text{M}}T$ curves reached a plateau at about 5 K, 15 K, and 40 K, respectively, corresponding to populating the triply degenerated excited states at $0.96, 2.37, \text{ and } 6.88 \text{ cm}^{-1}$, respectively.

The determination of J_{azido} highlights the difficulty in computing such subtle interactions within complex systems. To explain this difficulty, one may wonder about the

relevance of reducing the interactions between the triangular units with the interactions between the closest Cu^{II} ions of each unit. However, a more sophisticated treatment appears difficult in the BS-DFT framework, while WFT-based approaches would be untractable.

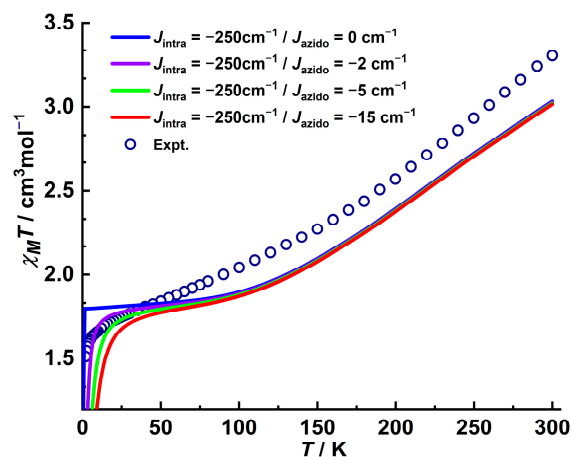


Figure 4. Calculated (solid lines) and experimental (filled circles) magnetic susceptibilities ($\chi_M T$) as a function of the temperature. Theoretical results are shown for an average J_{intra} of -250 cm^{-1} and different values for J_{azido} . Magnetic moments of Cu^{II} are obtained with the CASSCF method. Details of calculations are presented in Table S6.

4. Conclusions

Through synthetic engineering, for the first time, based on a triaminoguanidine ligand, we deliberately constructed a supramolecular $[\{\text{Cu}_3\text{L}(\mu\text{-N}_3)\}_4(\text{Py})_{14}] \cdot 2\text{Py}$ (**Cu₁₂**) metallacycle with four triangular sub-units. Each ligand traps three Cu^{II} ions in its tridentate-binding cavities (NNO), forming rigid planar triangular structures. This is also the first example of a higher nuclear compound in this metal–ligand combination that has been studied magnetically. While comparing **Cu₁₂** with reported spin-frustrated **Cu₃py** and **Cu₃bp** systems, similar strong antiferromagnetic interactions within the intra-triangular fragments can be observed and we can also expect spin frustration in **Cu₁₂**. This type of phenomenon in molecular systems is expected to give rise to spin–electric coupling, which allows for a manipulation of the molecular spin states. Hence, **Cu₁₂** can be seen as a potential candidate in the future for molecular spintronics.

Supplementary Materials: The following supporting information can be downloaded at: <https://www.mdpi.com/article/10.3390/magnetochemistry9050122/s1>, Figure S1: Molecular structure of **Cu₁₂**; Figure S2: Asymmetric unit of **Cu₁₂** in giving direction; Figure S3: Representation of copper environment geometries for **Cu₁₂**; Figure S4: Magnetization curve for **Cu₁₂** at 2 K; Table S1: Crystal data and structure refinement parameters for **Cu₁₂**; Table S2: Selected bond lengths (Å) and angles (°) for **Cu₁₂**; Table S3: Calculated geometries of **Cu₁₂** [75]; Table S4: Principal magnetic coupling constants (J in cm^{-1}) for **Cu₁₂** calculated at the DFT level with the B3LYP, B3LYP* and PBE0 functionals; Table S5: Calculated energy gap $\Delta E_{\text{ES1-GS}}$ (cm^{-1}) between the first excited state (ES1) and the ground state (GS), and the electronic g -factors for the ground state of the different metal centers in **Cu₁₂**; Table S6: Relative energy (in cm^{-1}) of the 20 lowest states of the spin Hamiltonian.

Author Contributions: Research design, data manipulation and writing original draft, B.A.; writing—review and editing, X.-L.L. and J.T.; theoretical calculations, G.D., F.G., O.C., W.P. and B.L.G.; supervising the project, J.T. project administration and funding acquisition, J.T. All authors have read and agreed to the published version of the manuscript.

Funding: This research was funded by National Natural Science Foundation of China; Chinese Academy of Sciences; Natural Science Foundation of Jilin Province of China; China Postdoctoral Science Foundation; Stratégie d’Attivité Durable.

Institutional Review Board Statement: Not applicable.

Informed Consent Statement: Not applicable.

Data Availability Statement: The data are available by corresponding authors.

Acknowledgments: We thank the National Natural Science Foundation of China (Grant 92261103), the Natural Science Foundation of Jilin Province of China (20200201244JC), the China Postdoctoral Science Foundation (2021M693397) and the Key Research Program of Frontier Sciences, CAS (Grant ZDBS-LY-SLH023) for financial support. X.-L. L. is thankful to the Chinese Academy of Sciences for a Special Research Assistant Grant (2021000162). B. A. is grateful for the support through CAS-TWAS President's Fellowship. G. D., F. G. and B. L. G. thank the French GENCI/IDRIS-CINES centers for high-performance computing resources and acknowledge the Stratégie d'Attivité Durable (SAD18006—LnCPLSMM) for financial support.

Conflicts of Interest: The authors declare no conflict of interest.

References

1. Leininger, S.; Olenyuk, B.; Stang, P.J. Self-Assembly of Discrete Cyclic Nanostructures Mediated by Transition Metals. *Chem. Rev.* **2000**, *100*, 853–908. [[CrossRef](#)]
2. Müller, I.M.; Robson, R. A New Class of Easily Obtained Carbonate-Related μ_3 -Ligands and a Protein-Sized Doughnut-Shaped Coordination Oligomer. *Angew. Chem. Int. Ed.* **2000**, *39*, 4357–4359. [[CrossRef](#)]
3. Buccella, D.; Lim, M.H.; Morrow, J.R. Metals in Biology: From Metallomics to Trafficking. *Inorg. Chem.* **2019**, *58*, 13505–13508. [[CrossRef](#)]
4. Holm, R.H.; Kennepohl, P.; Solomon, E.I. Structural and functional aspects of metal sites in biology. *Chem. Rev.* **1996**, *96*, 2239–2314. [[CrossRef](#)] [[PubMed](#)]
5. Brown, A.C.; Suess, D.L.M. An Open-Cuboidal $[\text{Fe}_3\text{S}_4]$ Cluster Characterized in Both Biologically Relevant Redox States. *J. Am. Chem. Soc.* **2023**, *145*, 2075–2080. [[CrossRef](#)] [[PubMed](#)]
6. Manicke, N.; Hoof, S.; Keck, M.; Braun-Cula, B.; Feist, M.; Limberg, C. A Hexanuclear Iron(II) Layer with Two Square-Planar FeO_4 Units Spanned by Tetrasiloxide Ligands: Mimicking of Minerals and Catalysts. *Inorg. Chem.* **2017**, *56*, 8554–8561. [[CrossRef](#)]
7. Nesterov, D.S.; Nesterova, O.V.; Pombeiro, A.J.L. Homo- and heterometallic polynuclear transition metal catalysts for alkane C-H bonds oxidative functionalization: Recent advances. *Coord. Chem. Rev.* **2018**, *355*, 199–222. [[CrossRef](#)]
8. Doroshenko, I.; Babiak, M.; Buchholz, A.; Tucek, J.; Plass, W.; Pinkas, J. Hexanuclear iron(III) alpha-aminophosphonate: Synthesis, structure, and magnetic properties of a molecular wheel. *New J. Chem.* **2018**, *42*, 1931–1938. [[CrossRef](#)]
9. Doroshenko, I.; Babiak, M.; Buchholz, A.; Görls, H.; Plass, W.; Pinkas, J. New molecular heptanuclear cobalt phosphonates: Synthesis, structures and magnetic properties. *New J. Chem.* **2018**, *42*, 9568–9577. [[CrossRef](#)]
10. Kostakis, G.E.; Perlepes, S.P.; Blatov, V.A.; Proserpio, D.M.; Powell, A.K. High-nuclearity cobalt coordination clusters: Synthetic, topological and magnetic aspects. *Coord. Chem. Rev.* **2012**, *256*, 1246–1278. [[CrossRef](#)]
11. Frost, J.M.; Harriman, K.L.M.; Murugesu, M. The rise of 3-d single-ion magnets in molecular magnetism: Towards materials from molecules? *Chem. Sci.* **2016**, *7*, 2470–2491. [[CrossRef](#)] [[PubMed](#)]
12. Liu, J.; Mrozek, J.; Ullah, A.; Duan, Y.; Baldoví, J.J.; Coronado, E.; Gaita-Ariño, A.; Ardavan, A. Quantum coherent spin–electric control in a molecular nanomagnet at clock transitions. *NatPh* **2021**, *17*, 1205–1209. [[CrossRef](#)]
13. Boudalis, A.K. Half-Integer Spin Triangles: Old Dogs, New Tricks. *Chem. Eur. J.* **2021**, *27*, 7022–7042. [[CrossRef](#)] [[PubMed](#)]
14. Cañón-Mancisidor, W.; Hermosilla-Ibáñez, P.; Spodine, E.; Paredes-García, V.; Gómez-García, C.J.; Espallargas, G.M.; Venegas-Yazigi, D. Slow Relaxation of the Magnetization on Frustrated Triangular Fe^{III} Units with $S = 1/2$ Ground State: The Effect of the Highly Ordered Crystal Lattice and the Counteranions. *Cryst. Growth Des.* **2021**, *21*, 6213–6222. [[CrossRef](#)]
15. Gangu, K.K.; Maddila, S.; Mukkamala, S.B.; Jonnalagadda, S.B. A review on contemporary Metal-Organic Framework materials. *Inorg. Chim. Acta* **2016**, *446*, 61–74. [[CrossRef](#)]
16. Chen, T.-H.; Popov, I.; Kaveevivitchai, W.; Miljanic, O.S. Metal-Organic Frameworks: Rise of the Ligands. *Chem. Mater.* **2014**, *26*, 4322–4325. [[CrossRef](#)]
17. Moulton, B.; Zaworotko, M.J. From molecules to crystal engineering: Supramolecular isomerism and polymorphism in network solids. *Chem. Rev.* **2001**, *101*, 1629–1658. [[CrossRef](#)]
18. Kitagawa, S.; Kitaura, R.; Noro, S.-i. Functional Porous Coordination Polymers. *Angew. Chem. Int. Ed.* **2004**, *43*, 2334–2375. [[CrossRef](#)]
19. Akintola, O.; Hornig, D.; Buchholz, A.; Görls, H.; Plass, W. Solvent-dependent selective cation exchange in anionic frameworks based on cobalt(II) and triphenylamine linkers: Reactor-dependent synthesis and sorption properties. *Dalton Trans.* **2017**, *46*, 8037–8050. [[CrossRef](#)]
20. Akintola, O.; Ziegenbalg, S.; Buchholz, A.; Görls, H.; Plass, W. A robust anionic pillared-layer framework with triphenylamine-based linkers: Ion exchange and counterion-dependent sorption properties. *CrystEngComm* **2017**, *19*, 2723–2732. [[CrossRef](#)]
21. Conerney, B.; Jensen, P.; Kruger, P.E.; MacGloinn, C. The 'Trinity' helix: Synthesis and structural characterisation of a C_3 -symmetric tris-bidentate ligand and its coordination to $\text{Ag}(\text{I})$. *Chem. Commun.* **2003**, *11*, 1274–1275. [[CrossRef](#)] [[PubMed](#)]

22. Kisets, I.; Gelman, D. Carbometalated Complexes Possessing Tripodal Pseudo- C_3 -Symmetric Triptycene-Based Ligands. *Organometallics* **2018**, *37*, 526–529. [[CrossRef](#)]
23. Lusby, P.J.; Müller, P.; Pike, S.J.; Slawin, A.M.Z. Stimuli-Responsive Reversible Assembly of 2D and 3D Metallosupramolecular Architectures. *J. Am. Chem. Soc.* **2009**, *131*, 16398–16400. [[CrossRef](#)]
24. Liu, Y.; Xuan, W.; Zhang, H.; Cui, Y. Chirality- and Threefold-Symmetry-Directed Assembly of Homochiral Octupolar Metal–Organoboron Frameworks. *Inorg. Chem.* **2009**, *48*, 10018–10023. [[CrossRef](#)] [[PubMed](#)]
25. Müller, I.M.; Möller, D. A New Ligand for the Formation of Triangular Building Blocks in Supramolecular Chemistry. *Eur. J. Inorg. Chem.* **2005**, *2005*, 257–263. [[CrossRef](#)]
26. Müller, I.M.; Spillmann, S.; Franck, H.; Pietschnig, R. Rational Design of the First Closed Coordination Capsule with Octahedral Outer Shape. *Chem. Eur. J.* **2004**, *10*, 2207–2213. [[CrossRef](#)]
27. Müller, I.M.; Möller, D.; Föcker, K. From a Monomer to a Protein-Sized, Doughnut-Shaped Coordination Oligomer—The Influence of Side Chains of C_3 -Symmetric Ligands in Supramolecular Chemistry. *Chem. Eur. J.* **2005**, *11*, 3318–3324. [[CrossRef](#)]
28. Müller, I.M.; Robson, R.; Separovic, F. A metallosupramolecular capsule with the topology of the tetrahedron, 3^3 , assembled from four guanidine-based ligands and twelve cadmium centers. *Angew. Chem. Int. Ed.* **2001**, *40*, 4385–4386. [[CrossRef](#)]
29. Oppel, I.M.; Föcker, K. Rational design of a double-walled tetrahedron containing two different C_3 -symmetric ligands. *Angew. Chem. Int. Ed.* **2008**, *47*, 402–405. [[CrossRef](#)]
30. Plass, W. Structural variety and magnetic properties of polynuclear assemblies based on 2-aminoglucose and tritopic triaminoguanidine ligands. *Coord. Chem. Rev.* **2009**, *253*, 2286–2295. [[CrossRef](#)]
31. Böhme, M.; Ion, A.E.; Kintzel, B.; Buchholz, A.; Görls, H.; Plass, W. Pentanuclear Nickel(II) Complex with two Vertex-Shared Triaminoguanidine Fragments and Symmetric Capping Ligand. *Z. Anorg. Allg. Chem.* **2020**, *646*, 999–1009. [[CrossRef](#)]
32. Zharkouskaya, A.; Görls, H.; Vaughan, G.; Plass, W. A new three-dimensional Cu(II) coordination polymer with triaminoguanidine building blocks. *Inorg. Chem. Commun.* **2005**, *8*, 1145–1148. [[CrossRef](#)]
33. Zharkouskaya, A.; Buchholz, A.; Plass, W. A new coordination polymer architecture with (10,3)-a network containing chiral hydrophilic 3-D channels. *Eur. J. Inorg. Chem.* **2005**, *2005*, 4875–4879. [[CrossRef](#)]
34. Plaul, D.; Böhme, M.; Ostrovsky, S.; Tomkowicz, Z.; Görls, H.; Haase, W.; Plass, W. Modeling Spin Interactions in a Triangular Cobalt(II) Complex with Triaminoguanidine Ligand Framework: Synthesis, Structure, and Magnetic Properties. *Inorg. Chem.* **2018**, *57*, 106–119. [[CrossRef](#)]
35. Böhme, M.; Schuch, D.; Buchholz, A.; Görls, H.; Plass, W. Spin Interactions and Magnetic Anisotropy in a Triangular Nickel(II) Complex with Triaminoguanidine Ligand Framework. *Z. Anorg. Allg. Chem.* **2020**, *646*, 166–174. [[CrossRef](#)]
36. Hamblin, J.; Tuna, F.; Bunce, S.; Childs, L.J.; Jackson, A.; Errington, W.; Alcock, N.W.; Nierengarten, H.; Van Dorselaer, A.; Leize-Wagner, E.; et al. Supramolecular Circular Helicates Formed by Destabilisation of Supramolecular Dimers. *Chem. Eur. J.* **2007**, *13*, 9286–9296. [[CrossRef](#)]
37. Kintzel, B.; Böhme, M.; Plaul, D.; Görls, H.; Yeche, N.; Seewald, F.; Klauss, H.-H.; Zvyagin, A.A.; Kampert, E.; Herrmannsdörfer, T.; et al. A Trinuclear High-Spin Iron(III) Complex with a Geometrically Frustrated Spin Ground State Featuring Negligible Magnetic Anisotropy and Antisymmetric Exchange. *Inorg. Chem.* **2023**, *62*, 3420–3430. [[CrossRef](#)]
38. Spielberg, E.T.; Gilb, A.; Plaul, D.; Geibig, D.; Hornig, D.; Schuch, D.; Buchholz, A.; Ardavan, A.; Plass, W. A Spin-Frustrated Trinuclear Copper Complex Based on Triaminoguanidine with an Energetically Well-Separated Degenerate Ground State. *Inorg. Chem.* **2015**, *54*, 3432–3438. [[CrossRef](#)]
39. Kintzel, B.; Böhme, M.; Liu, J.; Burkhardt, A.; Mrozek, J.; Buchholz, A.; Ardavan, A.; Plass, W. Molecular electronic spin qubits from a spin-frustrated trinuclear copper complex. *Chem. Commun.* **2018**, *54*, 12934–12937. [[CrossRef](#)]
40. Liu, J.; Mrozek, J.; Myers, W.K.; Timco, G.A.; Winpenny, R.E.P.; Kintzel, B.; Plass, W.; Ardavan, A. Electric Field Control of Spins in Molecular Magnets. *Phys. Rev. Lett.* **2019**, *122*, 037202. [[CrossRef](#)]
41. Ali, B.; Gendron, F.; Li, X.-L.; Le Guennic, B.; Tang, J. *Cis* and *Trans* Linkage of Spin Frustrated Copper Triangles Creating Cu_6 Clusters. *Chem. Sq.* **2020**, *4*, 4. [[CrossRef](#)]
42. Müller, I.M.; Möller, D.; Schalley, C.A. Rational design of tightly closed coordination tetrahedra that are stable in the solid state, in solution, and in the gas phase. *Angew. Chem. Int. Ed.* **2005**, *44*, 480–484. [[CrossRef](#)]
43. Sheldrick, G.M. Crystal structure refinement with SHELXL. *Acta Crystallogr. Sect. C Struct. Chem.* **2015**, *71*, 3–8. [[CrossRef](#)] [[PubMed](#)]
44. Sheldrick, G.M. SHELXT—Integrated space-group and crystal-structure determination. *Acta Crystallogr. Sect. A Found. Adv.* **2015**, *71*, 3–8. [[CrossRef](#)] [[PubMed](#)]
45. Bain, G.A.; Berry, J.F. Diamagnetic Corrections and Pascal’s Constants. *J. Chem. Educ.* **2008**, *85*, 532. [[CrossRef](#)]
46. Roos, B.O.; Taylor, P.R.; Sigbahn, P.E.M. A complete active space SCF method (CASSCF) using a density matrix formulated super-CI approach. *Chem. Phys.* **1980**, *48*, 157–173. [[CrossRef](#)]
47. Fdez. Galván, I.; Vacher, M.; Alavi, A.; Angeli, C.; Aquilante, F.; Autschbach, J.; Bao, J.J.; Bokarev, S.I.; Bogdanov, N.A.; Carlson, R.K.; et al. OpenMolcas: From Source Code to Insight. *J. Chem. Theory Comput.* **2019**, *15*, 5925–5964. [[CrossRef](#)]
48. Roos, B.O.; Lindh, R.; Malmqvist, P.-Å.; Veryazov, V.; Widmark, P.-O. Main Group Atoms and Dimers Studied with a New Relativistic ANO Basis Set. *J. Phys. Chem. A* **2004**, *108*, 2851–2858. [[CrossRef](#)]
49. Widmark, P.-O.; Malmqvist, P.-Å.; Roos, B.O. Density matrix averaged atomic natural orbital (ANO) basis sets for correlated molecular wave functions. *Theor. Chim. Acta* **1990**, *77*, 291–306. [[CrossRef](#)]

50. Douglas, M.; Kroll, N.M. Quantum electrodynamical corrections to the fine structure of helium. *Ann. Phys.-N. Y.* **1974**, *82*, 89–155. [[CrossRef](#)]
51. Hess, B.A. Applicability of the no-pair equation with free-particle projection operators to atomic and molecular structure calculations. *Phys. Rev. A* **1985**, *32*, 756–763. [[CrossRef](#)] [[PubMed](#)]
52. Hess, B.A. Relativistic electronic-structure calculations employing a two-component no-pair formalism with external-field projection operators. *Phys. Rev. A* **1986**, *33*, 3742–3748. [[CrossRef](#)] [[PubMed](#)]
53. Malmqvist, P.Å.; Roos, B.O.; Schimmelpfennig, B. The restricted active space (RAS) state interaction approach with spin-orbit coupling. *Chem. Phys. Lett.* **2002**, *357*, 230–240. [[CrossRef](#)]
54. Bolvin, H. An Alternative Approach to the g-Matrix: Theory and Applications. *Chemphyschem* **2006**, *7*, 1575–1589. [[CrossRef](#)] [[PubMed](#)]
55. Chibotaru, L.F.; Ungur, L. *Ab initio* calculation of anisotropic magnetic properties of complexes. I. Unique definition of pseudospin Hamiltonians and their derivation. *J. Chem. Phys.* **2012**, *137*, 064112. [[CrossRef](#)] [[PubMed](#)]
56. Fonseca Guerra, C.; Snijders, J.G.; te Velde, G.; Baerends, E.J. Towards an order-N DFT method. *Theor. Chem. Acc.* **1998**, *99*, 391–403. [[CrossRef](#)]
57. te Velde, G.; Bickelhaupt, F.M.; Baerends, E.J.; Fonseca Guerra, C.; van Gisbergen, S.J.A.; Snijders, J.G.; Ziegler, T. Chemistry with ADF. *J. Comput. Chem.* **2001**, *22*, 931–967. [[CrossRef](#)]
58. Baerends, A.J.A.; Atkins, E.J.Z.T.; Bashford, J.; Baseggio, D.; Bérces, O.; Bo, A.B.F.M.; Boerritger, C.; Cavallo, P.M.; Daul, L.; Chong, C.; et al. *ADF2017, SCM, Theoretical Chemistry*; Vrije Universiteit: Amsterdam, The Netherlands, 2017; Available online: <https://www.scm.com> (accessed on 1 January 2022).
59. van Lenthe, E.; Baerends, E.J.; Snijders, J.G. Relativistic regular two-component Hamiltonians. *J. Chem. Phys.* **1993**, *99*, 4597–4610. [[CrossRef](#)]
60. Ernzerhof, M.; Scuseria, G.E. Assessment of the Perdew–Burke–Ernzerhof exchange–correlation functional. *J. Chem. Phys.* **1999**, *110*, 5029–5036. [[CrossRef](#)]
61. Adamo, C.; Barone, V. Toward reliable density functional methods without adjustable parameters: The PBE0 model. *J. Chem. Phys.* **1999**, *110*, 6158–6170. [[CrossRef](#)]
62. Becke, A.D. Density-functional thermochemistry. III. The role of exact exchange. *J. Chem. Phys.* **1993**, *98*, 5648–5652. [[CrossRef](#)]
63. Lee, C.; Yang, W.; Parr, R.G. Development of the Colle–Salvetti correlation-energy formula into a functional of the electron density. *Phys. Rev. B* **1988**, *37*, 785–789. [[CrossRef](#)]
64. Vosko, S.H.; Wilk, L.; Nusair, M. Accurate spin-dependent electron liquid correlation energies for local spin density calculations: A critical analysis. *Can. J. Phys.* **1980**, *58*, 1200–1211. [[CrossRef](#)]
65. Stephens, P.J.; Devlin, F.J.; Chabalowski, C.F.; Frisch, M.J. *Ab Initio* Calculation of Vibrational Absorption and Circular Dichroism Spectra Using Density Functional Force Fields. *J. Phys. Chem.* **1994**, *98*, 11623–11627. [[CrossRef](#)]
66. Salomon, O.; Reiher, M.; Hess, B.A. Assertion and validation of the performance of the B3LYP* functional for the first transition metal row and the G2 test set. *J. Chem. Phys.* **2002**, *117*, 4729–4737. [[CrossRef](#)]
67. Van Lenthe, E.; Baerends, E.J. Optimized Slater-type basis sets for the elements 1–118. *J. Comput. Chem.* **2003**, *24*, 1142–1156. [[CrossRef](#)] [[PubMed](#)]
68. Noodleman, L. Valence bond description of antiferromagnetic coupling in transition metal dimers. *J. Chem. Phys.* **1981**, *74*, 5737–5743. [[CrossRef](#)]
69. Yamaguchi, K.; Fukui, H.; Fueno, T. Molecular Orbital (Mo) Theory for Magnetically Interacting Organic Compounds. *Ab-Initio* Mo Calculations of The Effective Exchange Integrals for Cyclophane-Type Carbene Dimers. *Chem. Lett.* **1986**, *15*, 625–628. [[CrossRef](#)]
70. Yamaguchi, K.; Takahara, Y.; Fueno, T.; Houk, K.N. Extended Hartree-Fock (EHF) theory of chemical reactions. *Theor. Chim. Acta* **1988**, *73*, 337–364. [[CrossRef](#)]
71. Fabrizi de Biani, F.; Ruiz, E.; Cano, J.; Novoa, J.J.; Alvarez, S. Magnetic Coupling in End-to-End Azido-Bridged Copper and Nickel Binuclear Complexes: A Theoretical Study. *Inorg. Chem.* **2000**, *39*, 3221–3229. [[CrossRef](#)]
72. Cabrero, J.; de Graaf, C.; Bordas, E.; Caballol, R.; Malrieu, J.-P. Role of the Coordination of the Azido Bridge in the Magnetic Coupling of Copper(II) Binuclear Complexes. *Chem. Eur. J.* **2003**, *9*, 2307–2315. [[CrossRef](#)] [[PubMed](#)]
73. Chastanet, G.; Guennic, B.L.; Aronica, C.; Pilet, G.; Luneau, D.; Bonnet, M.-L.; Robert, V. Tuning magnetic exchange using the versatile azide ligand. *Inorg. Chim. Acta* **2008**, *361*, 3847–3855. [[CrossRef](#)]
74. Le Guennic, B.; Robert, V. From magnetic molecules to magnetic solids: An *ab initio* expertise. *C R Chim.* **2008**, *11*, 650–664. [[CrossRef](#)]
75. Casanova, D.; Lluell, M.; Alemany, P.; Alvarez, S. The Rich Stereochemistry of Eight-Vertex Polyhedra: A Continuous Shape Measures Study. *Chem. Eur. J.* **2005**, *11*, 1479–1494. [[CrossRef](#)]

Disclaimer/Publisher’s Note: The statements, opinions and data contained in all publications are solely those of the individual author(s) and contributor(s) and not of MDPI and/or the editor(s). MDPI and/or the editor(s) disclaim responsibility for any injury to people or property resulting from any ideas, methods, instructions or products referred to in the content.